Branon search in hadronic colliders

J.A.R. Cembranos[1, 2], A. Dobado[2] and A. L. Maroto[2]

[1] Departamento de Estadística e Investigación Operativa III,
[2] Departamento de Física Teórica,
Universidad Complutense de Madrid, 28040 Madrid, Spain

ABSTRACT

In the context of the brane-world scenarios with compactified extra dimensions, we study the production of brane fluctuations (branons) in hadron colliders ($p\bar{p}$, pp and $e^{\pm}p$) in terms of the brane tension parameter f, the branon mass M and the number of branons N. From the absence of monojets events at HERA and Tevatron (run I), we set bounds on these parameters and we also study how such bounds could be improved at Tevatron (run II) and the future LHC. The single photon channel is also analyzed for the two last colliders.

PACS: 11.25Mj, 11.10Lm, 11.15Ex

1 Introduction

Since rigid objects do not exist in relativistic theories, it is clear that brane fluctuations must play a role in the so called brane world, proposed some years ago by Arkani-Hamed, Dimopoulos and Dvali (ADD scenarios [1]), where the Standard Model (SM) particles are confined to live in the world brane and only gravitons are free to move along the $D > 4$ dimensional bulk space (see [2] for recent reviews). This fact turns out to be particularly true when the brane tension scale f ($\tau = f^4$ being the brane tension) is much smaller than the D dimensional or fundamental gravitational scale M_D, i.e., $f << M_D$. In this case the only relevant low-energy modes of the ADD scenarios are the SM particles and branons which are the quantized brane oscillations. Branons can be understood as the (pseudo)Goldstone bosons corresponding to the spontaneous breaking of translational invariance in the bulk space produced by the presence of the brane. It has been pointed out that branons could solve some of the problems of the brane-world scenarios such as the divergent virtual contributions from the Kaluza-Klein tower at the tree level or non-unitarity of the graviton production cross-sections [3]. As Goldstone bosons, branons are in principle massless, but in the cases where the metric of the extra dimensions cannot be factorized, they can become massive [4, 5]. This is similar to the case of pions which, being the Goldstone bosons of the spontaneous breaking of chiral symmetry, acquire some mass due to the explicit breaking of the symmetry induced by the quark masses.

In previous works the different effective actions have been obtained, namely: the effective action for the SM fields on the brane, that for the branon self-interactions and finally that corresponding to the interaction between SM fields and branons [4]. In general, this branon effective action can be parameterized by the number of branons N, the tension scale f and the branon masses (for an explicit construction see [6]). Using the effective action it is possible to obtain the different Feynman rules, the amplitudes and finally the cross-sections for branon production from SM particles. In [7, 8, 9] the case of electron-positron colliders has been considered. By using the Large Electron-Positron Collider (LEP) data it is possible to set important bounds on the tension scale and on the branon mass for a given branon number. Other restrictions have also been set from astrophysical and cosmological considerations due to the fact that branon dark matter can present relevant abundances [10].

In this work we study branon production in hadron colliders and also in electron-proton colliders such as HERA. Most of these cross sections have been studied by Creminelli and Strumia for the massless branon case [9]. We reproduce their results and extend the analysis for an arbitrary branon mass. The paper is organized as follows: In Sec.II we shortly review the branon effective action. In Sec.III we consider the case of proton-(anti)proton colliders like Tevatron or the future Large Hadron Collider (LHC). In Sec.IV electron(positron)-proton colliders like HERA are studied. In Sec.V we show the main

results for the relevant examples and in Sec.VI we set the conclusions.

2 Effective action

The relevant effective action describing the low-energy interactions of SM particles and branons was derived in [7], where the necessary vertices are detailed. The branon effective action can be expanded according to the number of branon fields appearing in each term:

$$S_{eff}[\pi] = S^{(0)}_{eff}[\pi] + S^{(2)}_{eff}[\pi] + ... \tag{1}$$

where the zeroth-order term is just a constant and the second-order is just the free action:

$$S^{(2)}_{eff}[\pi] = \frac{1}{2}\int d^4x(\delta_{\alpha\beta}\partial_\mu\pi^\alpha\partial^\mu\pi^\beta - M^2_{\alpha\beta}\pi^\alpha\pi^\beta), \tag{2}$$

with $\pi^\alpha(x)$ the branon fields where $\alpha = 1, 2, ..., N$ and $M^2_{\alpha\beta}$ is the squared mass matrix which, without loss of generality, can be assumed to be diagonal. The effective action for the SM particles and their interactions with branons is given by

$$S_{SM\pi} = \int d^4x[\mathcal{L}_{\mathcal{SM}} + \frac{1}{8f^4}(4\delta_{\alpha\beta}\partial_\mu\pi^\alpha\partial_\nu\pi^\beta - \eta_{\mu\nu}M^2_{\alpha\beta}\pi^\alpha\pi^\beta)T^{\mu\nu}_{SM}], \tag{3}$$

where $\mathcal{L}_{\mathcal{SM}}$ is the SM Lagrangian and $T^{\mu\nu}_{SM}$ is the SM energy-momentum tensor defined as:

$$T^{\mu\nu}_{SM} = -(g^{\mu\nu}\mathcal{L}_{\mathcal{SM}} + 2\frac{\delta\mathcal{L}_{\mathcal{SM}}}{\delta g_{\mu\nu}})|_{g_{\mu\nu}=\eta_{\mu\nu}}, \tag{4}$$

where $g_{\mu\nu}$ is some arbitrary metric on the world brane and $\eta_{\mu\nu}$ is the Minkowski metric.

In this work we are interested in the interactions between quarks and gluons or photons. Thus, for Dirac fermions with masses m_q belonging to some representation of a gauge group, such as $U(1)_{em}$ or $SU(3)_c$, with generators T^a, the Lagrangian is

$$\mathcal{L}_q = \bar{q}(i\gamma^\mu D_\mu - m_q)q, \tag{5}$$

where the covariant derivative is defined as $D_\mu = \partial_\mu - hA^a_\mu T^a$, h being the appropriate gauge coupling. Thus the energy-momentum tensor is given by

$$\begin{aligned} T^{\mu\nu}_q = \frac{i}{4}(&\bar{q}(\gamma^\mu D^\nu + \gamma^\nu D^\mu)q - (D^\nu\bar{q}\gamma^\mu + D^\mu\bar{q}\gamma^\nu)q) \\ &-\eta^{\mu\nu}(i(\bar{q}\gamma^\rho D^\rho - D_\rho\bar{q}\gamma^\rho)q - 2m_q\bar{q}q), \end{aligned} \tag{6}$$

from where it is possible to find vertices such as $\pi\pi\bar{q}q$ and $\pi\pi\bar{q}qA$. For gauge fields A the appropriate Lagrangian for perturbation theory is:

$$\mathcal{L}_\mathcal{A} = -\frac{1}{4}F^{a\mu\nu}F^a_{\mu\nu} + \mathcal{L}_{\mathcal{FP}}, \tag{7}$$

where as usual $F^a_{\mu\nu} = \partial_\mu A^a_\nu - \partial_\nu A^a_\mu - hC^{abc}A^b_\mu A^c_\nu$ and $\mathcal{L}_{\mathcal{FP}}$ is the Fadeev-Popov Lagrangian including the gauge fixing and the ghost terms. The energy-momentum tensor is:

$$T^{\mu\nu}_A = F^a_{\rho\sigma}F^a_{\lambda\theta}(\eta^{\sigma\lambda}\eta^{\rho\mu}\eta^{\theta\nu} + \frac{1}{4}\eta^{\rho\lambda}\eta^{\sigma\theta}\eta^{\mu\nu}) + T^{\mu\nu}_{FP}, \tag{8}$$

from where we can obtain the $\pi\pi AA$, $\pi\pi AAA$ and $\pi\pi AAAA$ vertices.

Therefore, by using these energy-momentum tensors and the effective action above, it is possible to obtain the different Feynman rules involving branons. One important observation is that in all the vertices obtained above, branons appear always by pairs. In fact they interact in a way similar to gravitons since they couple to the energy momentum tensor. This can be seen by making the formal identification of the graviton field $h_{\mu\nu}$ which appear in linearized gravity with

$$h_{\mu\nu} \to -\frac{1}{\kappa f^4}(\delta_{\alpha\beta}\partial_\mu\pi^\alpha\partial_\nu\pi^\beta - \frac{1}{4}\eta_{\mu\nu}M_{\alpha\beta}\pi^\alpha\pi^\beta). \tag{9}$$

where $\kappa = 4\sqrt{\pi}/M_P$ and M_P the Planck mass. Of course the physical meaning is completely different for branons and gravitons. In any case branons are expected to be weakly interacting and then they will scape to detection. Hence their typical signature will be missing energy and momentum. Since branons are produced by pairs, the energy spectrum of any other particle present in the final state will be continuous. In the following sections we will study the production mechanisms relevant for the different hadronic colliders.

3 Proton-(anti)proton colliders

For the case of proton-antiproton colliders like Tevatron, the most important processes for branon production are quark-antiquark annihilation or gluon fusion giving a gluon and a branon pair; and (anti)quark-gluon interaction giving an (anti)quark and a branon pair. Therefore the expected experimental signal will be in both cases one monojet J and missing energy and momentum. This is a very clear signature that in principle can be easily identified. Another potentially interesting process is the quark-antiquark annihilation giving a photon and a branon pair. In this case the signature is one single photon and missing energy and momentum.

The Feynman diagrams contributing to the main subprocesses $q\bar{q} \to g\pi\pi$, $gg \to g\pi\pi$, $qg \to q\pi\pi$ and $\bar{q}g \to \bar{q}\pi\pi$ are shown in Fig. 1, Fig. 2 and Fig. 3.

From these diagrams and the Feynman rules coming from the effective action of the previous section, it is possible to obtain the differential cross section:

$$\frac{d\sigma(q\bar{q} \to g\pi\pi)}{dk^2dt} = \frac{4\alpha_s N}{3}\frac{(k^2-4M^2)^2}{184320f^8\pi^2\hat{s}^3tu}\sqrt{1-\frac{4M^2}{k^2}}(\hat{s}k^2+4tu)(2\hat{s}k^2+t^2+u^2), \tag{10}$$

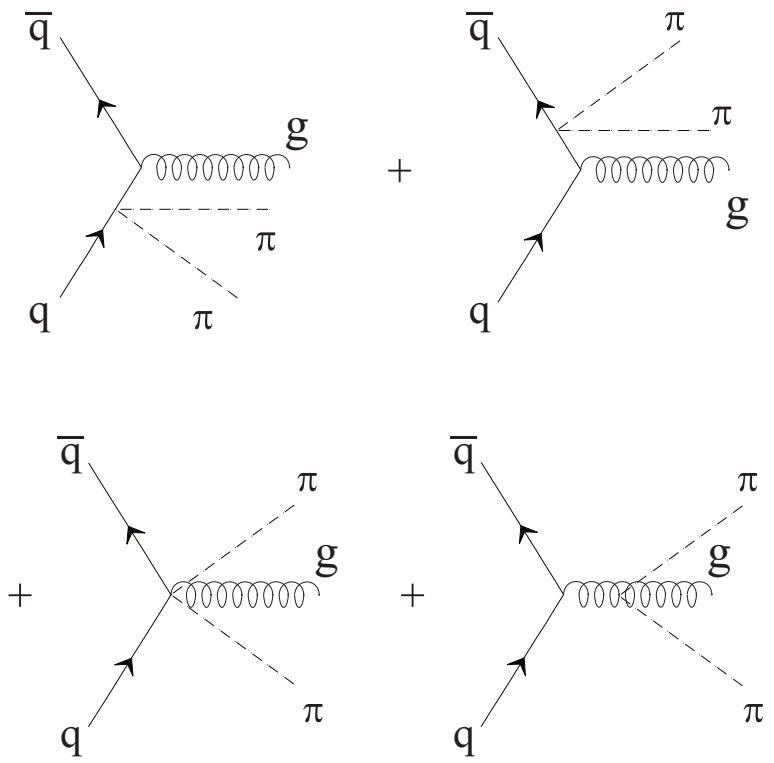

Figure 1: Feynman diagrams associated to the $q\bar{q} \to g\pi\pi$ subprocess.

where $\hat{s} \equiv (p_1 + p_2)^2$, $t \equiv (p_1 - q)^2$, $u \equiv (p_2 - q)^2$ and $k^2 \equiv (k_1 + k_2)^2$, p_1 and p_2 being the anti-quark and quark four-momenta respectively, q the gluon four-momentum and k_1 and k_2 the branon four-momenta. We have assumed for the sake of simplicity that all the branons are degenerated with a common mass M and that all the quarks are massless. We have also neglected the effects of the top quark. In addition we have the well-known relation $\hat{s}+t+u = k^2$. The contribution to the total cross section of the process $p\bar{p} \to g\pi\pi$ coming from this subprocess is given by

$$\sigma_{q\bar{q}}(p\bar{p} \to g\pi\pi) = \int_{x_{min}}^{1} dx \int_{y_{min}}^{1} dy \sum_{q} \bar{q}_{\bar{p}}(y;\hat{s}) q_p(x;\hat{s}) \int_{k^2_{min}}^{k^2_{max}} dk^2 \int_{t_{min}}^{t_{max}} dt \frac{d\sigma(q\bar{q} \to g\pi\pi)}{dk^2 dt} + ... \tag{11}$$

where $\bar{q}_{\bar{p}}(y;\hat{s})$ and $q_p(x;\hat{s})$ are the distribution functions of the anti-quark inside the antiproton and of the quark of flavor q inside the proton respectively, and x and y are the

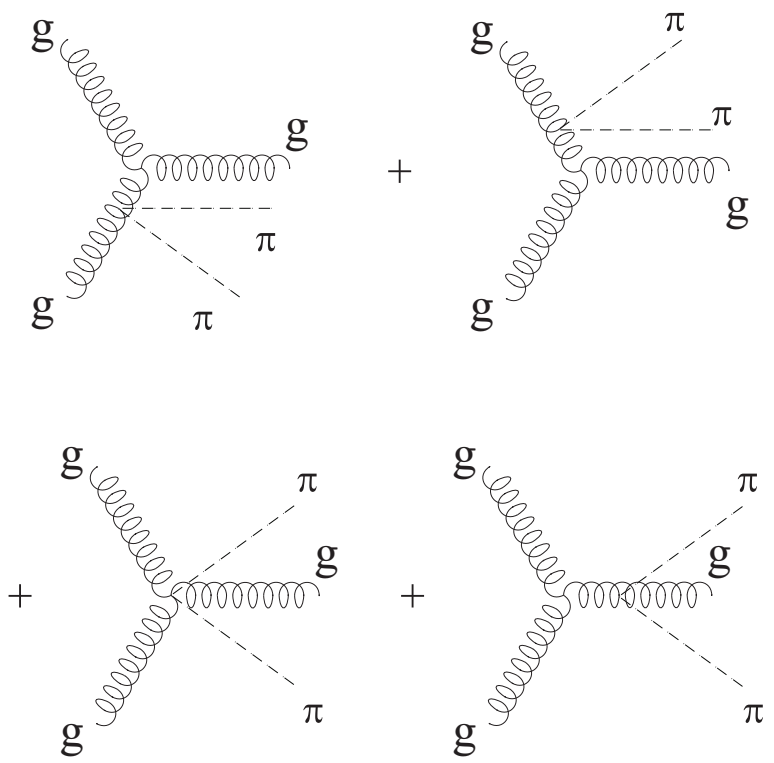

Figure 2: Feynman diagrams associated to the $gg \to g\pi\pi$ subprocess.

fractions of the proton and antiproton energy carried by the subprocess quark and anti-quark. The different limits of the integrals can be written in terms of the cuts used to define the total cross-section. For example, in order to be able to detect clearly the mono-jet one must impose a minimal value for its transverse energy E_T and a pseudorapidity range given by η_{min} and η_{max}. Then we have the limits $k^2_{min} = 4M^2$, $k^2_{max} = \hat{s}(1-2E_T/\sqrt{\hat{s}})$ and $t_{min(max)} = -(\hat{s} - k^2)[1 + \tanh(\eta_{min(max)})]/2$. On the other hand $x_{min} = s_{min}/s$ and $y_{min} = x_{min}/x$ where s is the total center of mass energy squared of the process and

$$s_{min} = 2E_T^2 + 4M^2 + 2E_T\sqrt{E_T^2 + 4M^2}. \tag{12}$$

In addition the dots in (11) represent the contribution of the case in which the quark comes from the antiproton and the anti-quark comes from the proton.

The cross-section of the subprocess $gg \to g\pi\pi$ is given by

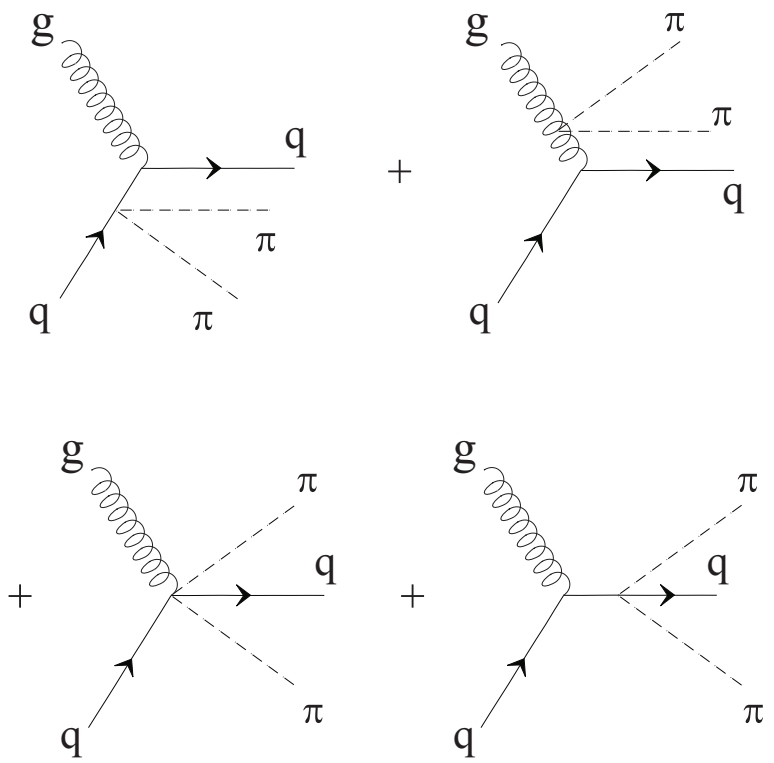

Figure 3: Feynman diagrams associated to the $qg \to q\pi\pi$ subprocess. The $\bar{q}g \to \bar{q}\pi\pi$ subprocess has the same diagrams, but changing the quark lines by the corresponding antiquark ones.

$$\frac{d\sigma(gg \to g\pi\pi)}{dk^2 dt} = \frac{\alpha_s N (k^2 - 4M^2)^2}{40960 f^8 \pi^2 \hat{s}^3 tu} \sqrt{1 - \frac{4M^2}{k^2}}$$
$$(\hat{s}^4 + t^4 + u^4 - k^8 + 6k^4(\hat{s}^2 + t^2 + u^2) - 4k^2(\hat{s}^3 + t^3 + u^3)), \tag{13}$$

where the Mandelstan variables are defined as in the previous case, with p_1 and p_2 being the initial gluon four-momenta, q the final gluon four-momentum and $k = k_1 + k_2$ the total branon four-momentum. Then the contribution to the total cross section from the $p\bar{p} \to g\pi\pi$ reaction is

$$\sigma_{gg}(p\bar{p} \to g\pi\pi) = \int_{x_{min}}^{1} dx \int_{y_{min}}^{1} dy g(y;\hat{s}) g(x;\hat{s})$$
$$\int_{k^2_{min}}^{k^2_{max}} dk^2 \int_{t_{min}}^{t_{max}} dt \frac{d\sigma(gg \to g\pi\pi)}{dk^2 dt}. \tag{14}$$

Here $g(x;s)$ is the gluon distribution function of the (anti)proton, x and y are the fractions

of the proton and antiproton energy carried by the initial gluons and the integration limits remain the same. From the above equations, it is possible to compute the total cross-section $\sigma(p\bar{p} \to g\pi\pi)$ in terms of the cut in the gluon (monojet) transverse energy E_T.

For the $qg \to q\pi\pi$ process the cross-section is given by

$$\frac{d\sigma(qg \to q\pi\pi)}{dk^2 dt} = -\frac{\alpha_s N}{2} \frac{(k^2 - 4M^2)^2}{184320 f^8 \pi^2 \hat{s}^3 tu} \sqrt{1 - \frac{4M^2}{k^2}} (uk^2 + 4t\hat{s})(2uk^2 + t^2 + \hat{s}^2), \quad (15)$$

with p_1 and p_2 being the quark and the gluon four-momenta respectively, q the final state quark four-momentum and k_1 and k_2 the branon four-momenta. The Mandelstam variables are defined as in previous cases. The cross-section for the conjugate process $\bar{q}g \to \bar{q}\pi\pi$ is exactly the same. Then the total cross section for the the reaction $p\bar{p} \to q\pi\pi$ is

$$\sigma(p\bar{p} \to q\pi\pi) = \int_{x_{min}}^{1} dx \int_{y_{min}}^{1} dy \sum_q g(y;\hat{s}) q_p(x;\hat{s}) \int_{k^2_{min}}^{k^2_{max}} dk^2 \int_{t_{min}}^{t_{max}} dt \frac{d\sigma(qg \to q\pi\pi)}{dk^2 dt} + ... \quad (16)$$

In this equation x and y are the fractions of the proton and antiproton energy carried by the subprocess quark and gluon. The different integration limits are defined as in the previous case in terms of the minimal transverse energy of the quark (monojet) E_T and the dots refer to the case where the initial gluon is coming from the proton and the quark is coming from the antiproton. In addition we have the contribution from the conjugate case where we take an anti-quark from the proton and a gluon from the antiproton and conversely. This amount just to a factor of two.

From all the above equations it is possible to compute the total cross-section $\sigma(p\bar{p} \to J\pi\pi)$ in terms of the cut in the jet transverse energy E_T.

For the subprocess $q\bar{q} \to \gamma\pi\pi$ the cross-section is given by

$$\frac{d\sigma(q\bar{q} \to \gamma\pi\pi)}{dk^2 dt} = \frac{Q_q^2 \alpha N (k^2 - 4M^2)^2}{184320 f^8 \pi^2 \hat{s}^3 tu} \sqrt{1 - \frac{4M^2}{k^2}} (\hat{s}k^2 + 4tu)(2\hat{s}k^2 + t^2 + u^2). \quad (17)$$

Here the notation is similar to the $q\bar{q} \to g\pi\pi$ case with the obvious differences in couplings, color and charge factors. Thus

$$\sigma(p\bar{p} \to \gamma\pi\pi) = \int_{x_{min}}^{1} dx \int_{y_{min}}^{1} dy \sum_q \bar{q}_{\bar{p}}(y;\hat{s}) q_p(x;\hat{s}) \int_{k^2_{min}}^{k^2_{max}} dk^2 \int_{t_{min}}^{t_{max}} dt \frac{d\sigma(q\bar{q} \to \gamma\pi\pi)}{dk^2 dt} + ... \quad (18)$$

All the previous discussion about branon production in $p\bar{p}$ reactions can be easily translated to the pp case. The only point is to change the antiproton distribution functions of the different partons by the corresponding proton ones.

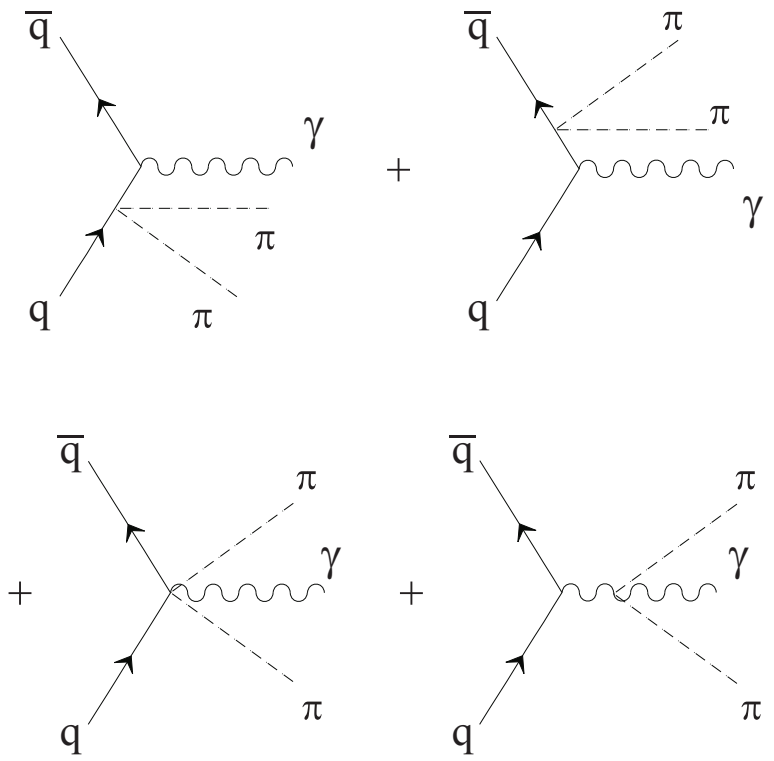

Figure 4: Feynman diagrams associated to the $q\bar{q} \to \gamma\pi\pi$ subprocess.

4 Electron(positron)-proton colliders

For electron(positron)-proton colliders like HERA, the most interesting branon creating process is branon photoproduction, where a photon emitted by the electron(positron) interacts with a quark(antiquark) from the proton giving a quark (antiquark) and a branon pair. Thus the experimental signature is again one monojet J plus missing energy and momentum. The relevant Feynman diagrams are shown in Fig. 5 and the corresponding differential cross-section for the subprocess $\gamma q \to q\pi\pi$ is

$$\frac{d\sigma(\gamma q \to q\pi\pi)}{dk^2 dt} = -\frac{3Q_q^2 \alpha N (k^2 - 4M^2)^2}{184320 f^8 \pi^2 \hat{s}^3 tu} \sqrt{1 - \frac{4M^2}{k^2}} (uk^2 + 4t\hat{s}^2)(2uk^2 + t^2 + \hat{s}^2), \quad (19)$$

where $\hat{s} = (p+q)^2, t = (p-k)^2$ and $u = (q-k)^2$, p being the photon, q the proton quark, q' the final quark and k the total branon momenta respectively. The total cross-section

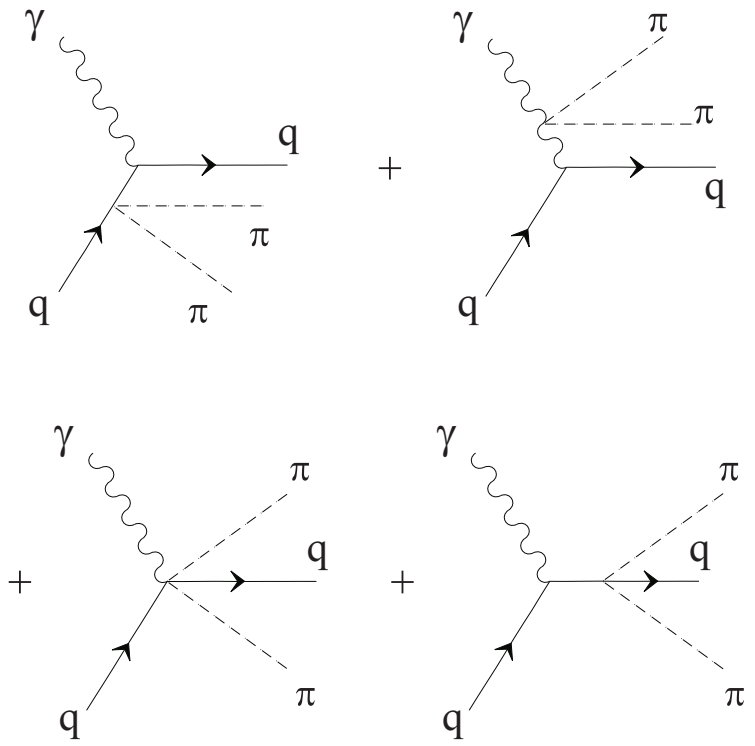

Figure 5: Feynman diagrams associated to the $q\gamma \to q\pi\pi$ subprocess. The $\bar{q}\gamma \to \bar{q}\pi\pi$ subprocess has the same diagrams but changing the quark lines by the corresponding antiquark ones.

for the process $e^{\pm}p \to q\pi\pi$ is given by

$$\sigma(e^{\pm}p \to q\pi\pi) = \int_{x_{min}}^{1} dx \int_{y_{min}}^{1} dy \sum_{q} F(y) q_p(x;\hat{s}) \int_{k^2_{min}}^{k^2_{max}} dk^2 \int_{t_{min}}^{t_{max}} dt \frac{d\sigma(\gamma q \to q\pi\pi)}{dk^2 dt}, \tag{20}$$

x and y are defined in this case as $q = xP_p$ and $P = yP_e$ with P_p and P_e being the proton and electron(positron) momenta respectively. Thus at high energies compared with the proton mass $\hat{s} = xys$ where $s = (P_e + P_p)^2$. The integral limits y_{min}, x_{min}, $k^2_{min,max}$ and $t_{min,max}$ are defined like in the proton-(anti)proton collider case.

The photon spectrum $F(y)$ can be obtained from the well-known Weizsäcker-Williams approximation [11]:

$$F(y) = \frac{\alpha}{2\pi y}[1 + (1-y)^2] \log \frac{s'}{4m_e^2}, \tag{21}$$

with $s' = xs$ and m_e being the electron mass.

The cross-section $\sigma(e^{\pm}p \to \bar{q}\pi\pi)$ can be obtained in a similar way. Then the total contribution to monojet plus missing energy and momentum production for large enough E_T coming from branons can be written as the sum of $\sigma(e^{\pm}p \to q\pi\pi)$ and $\sigma(e^{\pm}p \to \bar{q}\pi\pi)$.

5 Results

By using the cross-sections shown in the previous sections it is possible to compute the expected number of branon pairs produced in the different hadron colliders in terms of the brane tension parameter f, the branon mass M and the number of branons N. To this end we have used the distribution functions which can be found in [12]. The values of the electromagnetic and strong couplings have been taken at the electroweak boson masses, namely $\alpha = 0.0781$ and $\alpha_s = 0.1171$. However our final results do not depend too much on the precise value of these couplings. In fact our main source of error is the use of an effective action to describe the SM particles and branon interactions since, in principle, this is only guaranteed for energies well below $4\pi f$.

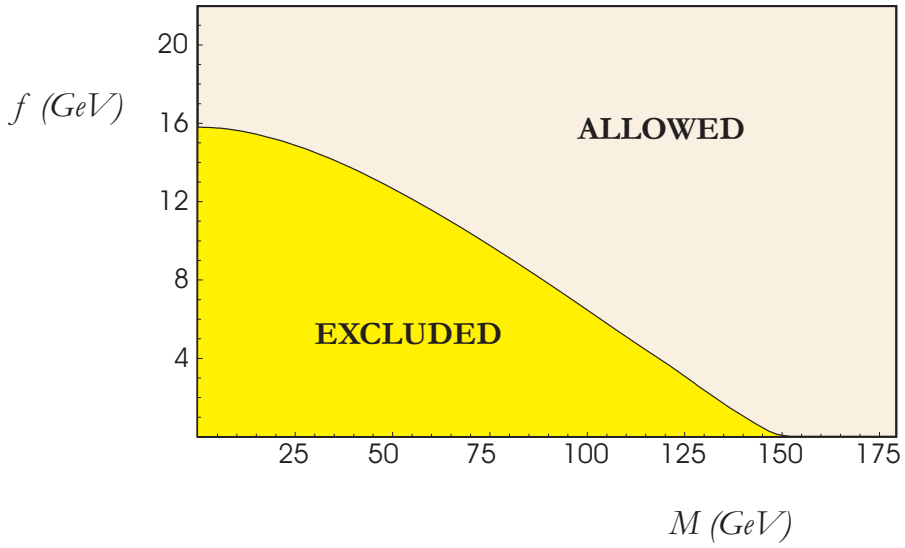

Figure 6: Exclusion region at the 95 % c.l. in the parameter space $f - M$ for $N = 1$ from ZEUS data on jet production.

As discussed in the introduction, our main goal in this work is to study the bounds that can be set on the f, M and N parameters coming from hadron colliders. We will present all our limits at the 95% confidence level. In particular, for the electron(positron)-proton case, HERA is the most relevant experiment. In fact, the ZEUS collaboration has studied the jet production in charged current deep inelastic $e^{+}p$ scattering. Its results

are perfectly compatible with the SM background and therefore, we can set some bounds on the branon production and hence on the f, M and N parameters. These data were taken from 1995 to 2000 at a maximum CM energy of 318 GeV. The total integrated luminosity was 110.5 pb^{-1} and the cuts on the pseudorapidity and the transverse energy were $-1 \leq \eta \leq 2$ and $E_T \geq 14$ GeV (see [13] for more details). By using the same cuts with our cross-sections for monojet plus a branon pair production, we find the bound $f > 16N^{1/8}$ GeV for massless branons. For a branon mass larger than 152 GeV there is no restrictions on the f value because of kinematical reasons. For the intermediate M values the bounds obtained can be seen in Fig. 6 where we have assumed $N = 1$. For other N values one just has to take into account that the bound scales like $N^{-1/8}$ since all the cross-sections are proportional to Nf^{-8}.

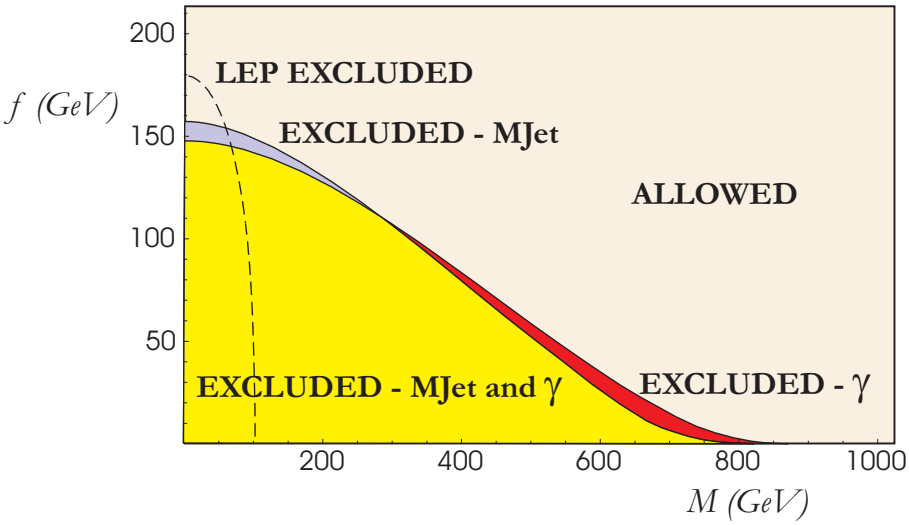

Figure 7: Exclusion region $f - M$ at the 95 % c.l. for $N = 1$ with $D\emptyset$ data in the monojet channel, and with CDF data in the single photon channel. The dashed line corresponds to the LEP-II limits obtained by the L3 collaboration using single-photon data [8]

In the $p\bar{p}$ case the most relevant experimental information so far is the one obtained at the Tevatron (Run I). The $D\emptyset$ detector has studied the monojet channel and CDF the single photon one. As far as the number of events found in both cases is compatible with the SM background, we can set new bounds on the branon theory parameters. For light branons the most important bound comes from the $D\emptyset$ data. These data were taken from 1994 to 1996 at a CM energy of 1.8 TeV and correspond to an integrated luminosity 78.8 ± 3.9 pb^{-1}. The cuts on the pseudorapidity and the transverse energy were $|\eta| \leq 1$ and $E_T \geq 150$ GeV (see [14] for the details of the analysis). The total number of monojets observed was 38 and the expected number from the SM plus cosmic rays events was 38 ± 9.6. By using our cross sections for monojet plus a branon pair

production with these cuts we get the bound $f > 157N^{1/8}$ GeV for light branons. The restrictions for f improve up to a branon mass of 822 GeV. For the intermediate M values the bounds obtained can be seen in Fig. 7 for $N = 1$.

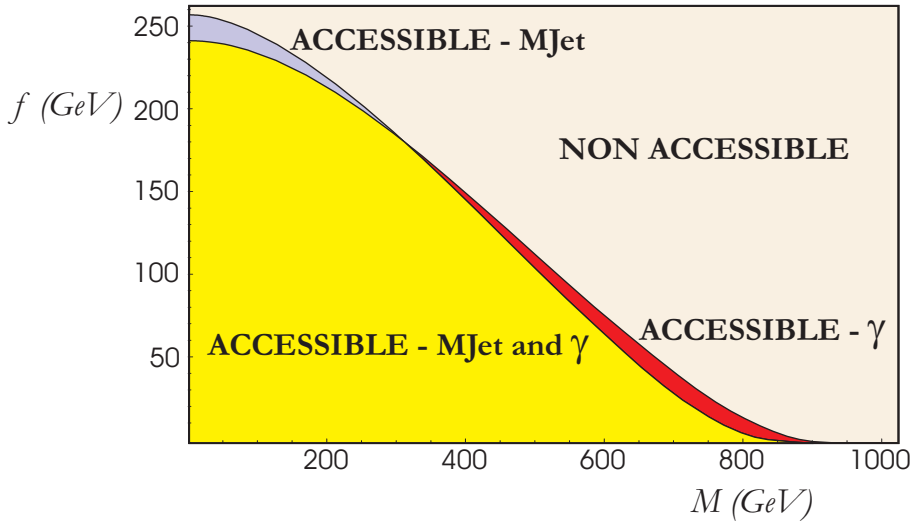

Figure 8: Sensitivity estimation at the 95 % c.l. for the second run of Tevatron in the parameter space $f - M$ for $N = 1$.

In a similar way we can use the CDF data on single photon production. In this case the total luminosity collected was 87 ± 4 pb^{-1} and the pseudorapidity cut was $|\eta| \leq 1$. For the transverse photon energy several cuts were considered (for example 55 GeV at the 75% efficiency). The total expected background for this process was 11.0 ± 2.2, without taking into account the QCD contribution (see [15] for the details of the analysis), and the number of events found was 11. Comparing this result with our computations for photon plus one branon pair production, we find the bound $f > 148N^{1/8}$ GeV for massless branons and no bound for M larger than 872 GeV. The bound obtained for the rest of the cases is shown also in Fig. 7.

In addition to this analysis corresponding to the Tevatron data (Run I), it is also interesting to make some estimation about the bounds that could be set from future experiments such as Tevatron (Run II) and the LHC. In the case of the Tevatron (Run II), which is already in progress, the main novelties are a CM energy which equals 1.96 TeV and an expected integrated luminosity $\mathcal{L}_{II}$ at the end of the run of about 200 pb^{-1}. The detectors are also improved so that the pseudorapidity cuts can be taken as $|\eta| \leq 3$ for $D\emptyset$ and $|\eta| \leq 3.6$ for CDF. This would result in a factor of $\sqrt{\mathcal{L}_{II}/\mathcal{L}_{I}}$ on the statistical significance when compared to the Run I, with integrated luminosity $\mathcal{L}_{I}$, provided that the CM energy and the cuts were the same. For massless branons, the bound on f scales

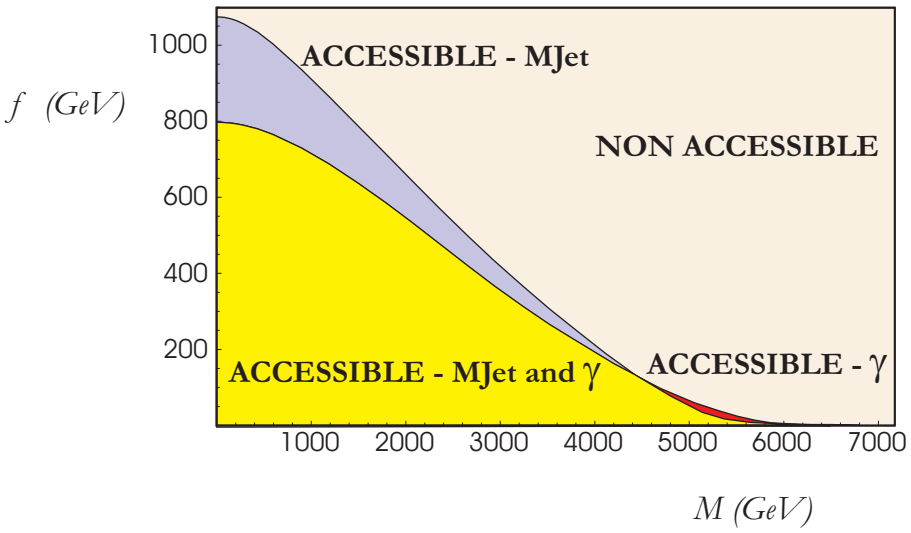

Figure 9: Sensitivity estimation at the 95 % c.l. for the LHC in the $f - M$ plane for $N = 1$.

as the CM energy $E_{CM}^{3/4}$. Even more important is the possibility of exploring higher branon masses, since the kinematical limit is given by $M_0 = \sqrt{E_{CM}^2 - 2E_{CM}E_T}/2$. In Fig. 8 we show the expected bounds from the Run II in the $f - M$ plane, again for $N = 1$.

The LHC will produce pp collisions at a CM energy of 14 TeV and the integrated luminosity will be something about 10^5 pb^{-1}. In order to estimate the bounds on the f, M and N parameters that will be possible to obtain at the LHC, we have proceeded in a similar way as in the Tevatron case, with the obvious changes in the distribution functions due to the fact that now we are dealing with pp instead of $p\bar{p}$ collisions. We have kept the same cuts except for the transverse energy which has been corrected in order to maintain the same proportion relative to the CM energy. Again the best bounds for f come from monojet production, which for $M = 0$ turns out to be $f > 1075N^{1/8}$ GeV. For low f the best bound for M is given by the single photon channel ($M_0 = 6781$). The LHC sensitivity for other values in the $f - M$ plane can be found in Fig. 9 for $N = 1$.

6 Conclusions

In this work we have studied the flexible brane-world scenario, where the brane tension scale f is much smaller than the fundamental D-dimensional gravitational scale M_D. In this case, the relevant low-energy degrees of freedom are the SM particles and the brane fluctuations or branons. From the corresponding effective action, we have calculated the relevant cross-sections for different branon searches in hadronic colliders. We have

used the information coming from HERA and the first Tevatron Run in order to get different exclusion plots on the branon mass M and the tension scale f plane for a given branon number N. Monojet production turns out to be the most efficient process for light branons, whereas the single photon channel is the most important one for heavy branons.

Exper.	$\sqrt{s}$(TeV)	$\mathcal{L}$(pb^{-1})	E_T(GeV)	$\eta_{min,max}$	σ_0(GeV^{-2})	f_0(GeV)	M_0(GeV)
HERA [1]	0.318	110.5	14	-1, 2	$7.0\,10^{-7}$	16	152
Teva-I [1]	1.8	78	150	-1, 1	$6.3\,10^{-10}$	157	822
Teva-I [2]	1.8	87	55	-1.1, 1.1	$1.3\,10^{-10}$	148	872
Teva-II [1]	1.96	10^3	150	-3, 3	$3.2\,10^{-10}$	256	902
Teva-II [2]	1.96	10^3	55	-3.6, 3.6	$7.0\,10^{-11}$	240	952
LHC [1]	14	10^5	1000	-3, 3	$1.8\,10^{-11}$	1075	6481
LHC [2]	14	10^5	430	-3.6, 3.6	$3.8\,10^{-12}$	797	6781

Table 1: Summary of the main characteristics of the analysis performed for hadronic colliders. All the results are presented at the 95 % c.l. We have studied two channels: the one marked with an upper index [1] is related to monojet production, whereas the single photon is labelled with an upper index [2]. We considered four different experiments: HERA, the I and II Tevatron runs and the LHC. Obviously the data corresponding to the two last experiments are estimations, whereas the first two analysis have been performed with real data. $\sqrt{s}$ is the center of mass energy associated to the total process; $\mathcal{L}$ is the total integrated luminosity; E_T is the transverse energy cut; $\eta_{min,max}$, the pseudorapidity limits; σ_0 is the estimation for the cross section sensitivity limit; f_0, the bound in the brane tension scale for one massless branon ($N = 1$) and M_0 the limit on the branon mass for $f = 0$.

We have also extended the analysis to future hadronic colliders. The corresponding sensitivity regions for the second Tevatron run and the LHC have also been plotted (see Table 1 for a summary of the analysis).

These analysis improve those already done for electron-positron colliders for heavy branons, whereas for light branons, the results are similar [7, 8, 9]. The Tevatron (run I) limit $M_0 = 872$ GeV can be compared to the analogous limit from LEP II $M_0 = 103$ GeV [8]. According to the previous estimations, the Tevatron run II could also improve the bound $f_0 = 180$ GeV obtained by LEP-II. On the other hand, LHC could detect branons up to a mass of several TeV ($M_0 = 6781$ GeV) improving even the CLIC prospects ($M_0 \simeq 2500$ GeV) [7].

The study of branons in colliders can be complemented with other bounds coming from astrophysics and cosmology (see Fig. 10). In fact, as shown in [10], the branon relic abundance can have cosmological consequences. Other issues related to branon phenomenology, such as their radiative corrections to the SM processes, or their distinctive signatures at colliders with respect to the KK gravitons will be analyzed elsewhere.

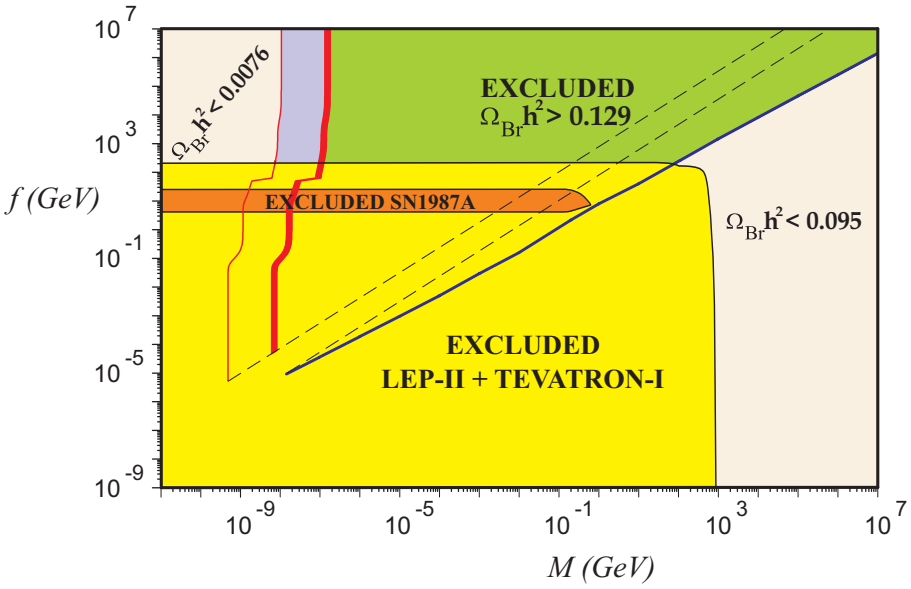

Figure 10: Relic abundance in the $f - M$ plane for a model with one branon of mass: M. The two lines on the left correspond to the $\Omega_{Br}h^2 = 0.0076$ and $\Omega_{Br}h^2 = 0.129 - 0.095$ curves for hot-warm relics, whereas the right line corresponds to the latter limits for cold relics (see [10] for details). The lower area is excluded by single-photon processes at LEP-II [8] together with monojet signal at Tevatron-I. The astrophysical constraints are less restrictive and they mainly come from supernova cooling by branon emission [10].

Note added: After this paper was completed, we were informed by M. Spiropulu that CDF collaboration had performed a monojet study [16] which could improve the bounds in a more detailed analysis.

Acknowledgements: We would like to thank J. Terrón, M. Vázquez and M. Spiropulu for useful comments and experimental information. This work has been partially supported by the DGICYT (Spain) under the project numbers FPA2000-0956 and BFM2002-01003.

References

[1] N. Arkani-Hamed, S. Dimopoulos and G. Dvali, *Phys. Lett.* **B429**, 263 (1998); N. Arkani-Hamed, S. Dimopoulos and G. Dvali, *Phys. Rev.* **D59**, 086004

(1999); I. Antoniadis *et al.*, *Phys. Lett.* **B436** 257 (1998)

[2] A. Perez-Lorenzana, *AIP Conf.Proc.* **562** 53 (2001); V.A. Rubakov, *Phys.Usp.* **44** (2001) 871, *Usp.Fiz.Nauk* **171** 913 (2001); Y. A. Kubyshin hep-ph/0111027; C. Csaki hep-ph/0404096

[3] M. Bando *et al.*, *Phys. Rev. Lett.* **83**, 3601 (1999)

[4] R. Sundrum, *Phys. Rev.* **D59**, 085009 (1999); A. Dobado and A.L. Maroto *Nucl. Phys.* **B592**, 203 (2001)

[5] J.A.R. Cembranos, A. Dobado and A.L. Maroto, *Phys. Rev.* **D65**, 026005 (2002); J.A.R. Cembranos, A. Dobado and A.L. Maroto, hep-ph/0107155

[6] A.A. Adrianov *et al.*, *J. High Energy Phys.* **07**, 063 (2003)

[7] J. Alcaraz *et al. Phys. Rev.* **D67**, 075010 (2003); J.A.R. Cembranos, A. Dobado, A. L. Maroto, *AIP Conf.Proc.* **670**, 235 (2003)

[8] P. Achard *et al.*, L3 Collaboration, *Phys. Lett.* **B597**, 145 (2004)

[9] P. Creminelli and A. Strumia, *Nucl. Phys.* **B596**, 125 (2001)

[10] J.A.R. Cembranos, A. Dobado and A.L. Maroto, *Phys. Rev. Lett.* **90**, 241301 (2003); T. Kugo and K. Yoshioka, *Nucl. Phys.* **B594**, 301 (2001); J.A.R. Cembranos, A. Dobado and A.L. Maroto, *Phys. Rev.* **D68**, 103505 (2003); A.L. Maroto, *Phys. Rev.* **D69**, 043509 (2004); J.A.R. Cembranos, A. Dobado and A.L. Maroto, hep-ph/0307015 and hep-ph/0402142; A.L. Maroto, *Phys. Rev.* **D69**, 101304 (2004); AMS Collaboration, AMS Internal Note 2003-08-02

[11] C. von Weizsäcker and F.J. Williams *Z. Phys.* **88**, 612 (1934)

[12] A.D. Martin *et al.*, *Eur. Phys. J. C* **4** (1998) 463
H.L. Lai *et al.*, hep-ph/9903282, http://durpdg.dur.ac.uk

[13] S. Chekanov *et al.*, *ZEUS* Collaboration, *Eur. Phys. J* **C31**, 149 (2003); M.L. Vazquez, "Jet Production in Charged Current Deep Inelastic Scattering at HERA" *Doctoral Thesis* (Madrid, Autonoma U., Dept. Theor. Phys.), DESY-THESIS-2003-006, Dec 2002.

[14] V. M. Abazov *et al.*, *DØ* Collaboration, *Phys. Rev. Lett.* **90**, 251802 (2003)

[15] D. Acosta *et al.*, *CDF* Collaboration, *Phys. Rev. Lett.* **89**, 281801 (2002)

[16] D. Acosta *et al.*, *CDF* Collaboration *Phys. Rev. Lett.* **92**, 121802 (2004)